OPTIMIZATION OF THE GRAPHITIZATION PROCESS AT AGE-1

Mojmír Němec[1,2,3] • Lukas Wacker[2] • Heinz Gäggeler[1]

ABSTRACT. The reaction conditions for the graphitization of CO_2 with hydrogen were optimized for a fast production of high-quality carbon samples for accelerator mass spectrometry (AMS) measurement. The iron catalyst in use is first oxidized by heating with air to remove possible carbon and other impurities and then after evacuation reduced back to iron with hydrogen in several flushing steps to remove any iron oxide. The optimum conditions for a fast graphitization reaction were experimentally determined by changing the reaction temperatures and the H_2/CO_2 ratio. The resulting graphite samples were measured by AMS to find the smallest isotopic changes ($\delta^{13}C$) at a minimum of molecular fragment formation (^{13}CH current). The improvements are based on thermodynamic data and are explained with Baur-Glaessner diagrams.

INTRODUCTION

Graphitization of samples is a standard procedure for high-precision accelerator mass spectrometry (AMS) ^{14}C measurement. In the past, several types of graphitization systems were developed and used in routine sample preparation. In spite of the many routinely operating graphitization lines, only few laboratories present their operational conditions and efficiency (Dee and Ramsey 2000; Yoneda et al. 2004; Santos et al. 2007). The graphitization process is not yet fully understood; therefore, a high potential still exists to improve the carbon production by changing the various reaction parameters.

The graphitization reactions were investigated many years ago (Manning and Reid 1977; Sacco and Reid 1979; Sacco et al. 1984), but with no direct relation to AMS needs. These reactions were later adapted for AMS (Vogel et al. 1984, 1987b) and since then commonly used. Besides the reduction of CO_2 with hydrogen on the iron, nickel, or cobalt surfaces, other reducing agents like Mn, Zn, or TiH are used (Jull et al. 1986; Slota et al. 1987; Verkouteren et al. 1997; Vogel 1992; Vogel et al. 1987a; Xu et al. 2007). McNichol et al. (1992) investigated the gas phase composition during the H_2 and Fe/Zn reduction systems, but there are a limited number of publications focused on the reaction system, its reactions and conditions.

Here, the reactions of carbon oxides with hydrogen or water on the Fe surface (Bosch reaction, Fischer-Tropsch synthesis, water gas reaction) were studied with the automated graphitization equipment (AGE) (Wacker et al. 2010) that was developed at ETH Zurich to prepare fast and efficiently samples for radiocarbon measurement. Samples are combusted in a standard elemental analyzer (EA; Elementar, Vario Micro Cube) and the resulting CO_2 is absorbed in a zeolite trap. The CO_2 is released by heating the trap and expands to the individual reactors, where it is reduced by H_2 to graphite on the surface of iron catalyst. The use of liquid nitrogen is avoided. The carbon samples are routinely measured at a small 200kV AMS device (MICADAS) (Synal et al. 2007), where only the 1+ ionic state is used. Optimization of the sample preparation was made with respect to MICADAS needs for stable, high-precision measurement.

[1]Department for Chemistry and Biochemistry, Universität Bern, Freiestrasse 3, CH-3012 Bern, Switzerland.
[2]Laboratory of Ion Beam Physics, HPK, Schafmattstrasse 20, CH-8093 Zürich, Switzerland.
[3]Department of Nuclear Chemistry, Czech Technical University, in Prague, Brehova 7, 115 19 Prague 1, Czech Republic, Corresponding author. Email:mojmir.nemec@fjfi.cvut.cz.

Proceedings of the 20th International Radiocarbon Conference, edited by A J T Jull
RADIOCARBON, Vol 52, Nr 2–3, 2010, p 1380–1393

INSTRUMENTAL SETUP AND PROCEDURE

The AGE has already been described elsewhere (Wacker et al. 2010). The main advantage of this device is a zeolite absorption column (trap) used for CO_2 transport and concentration. Operating software (Figure 1) written in LabVIEW allows precise setting of the parameters for oven temperatures, reactor filling, and timing. Temperatures and pressures are logged during graphitization.

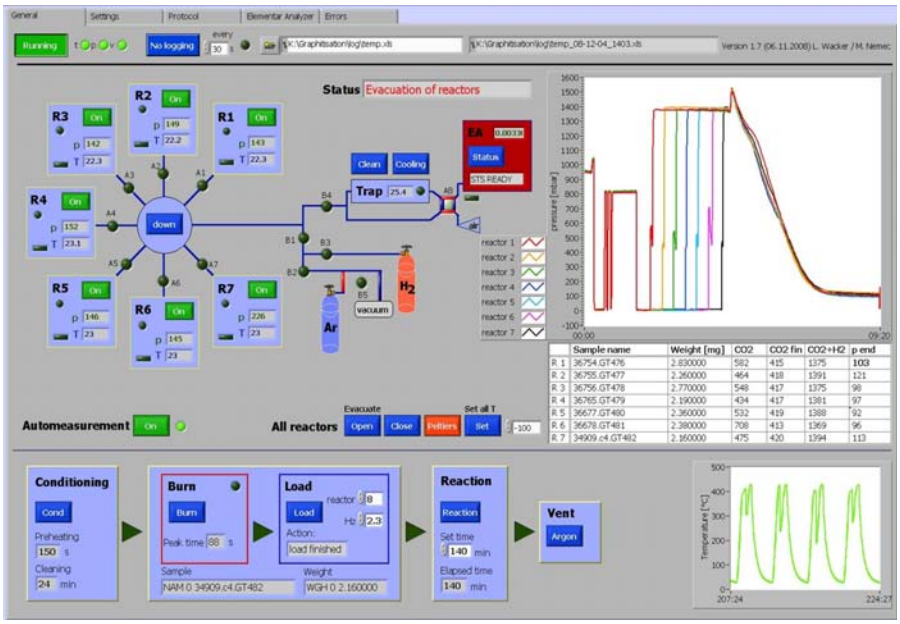

Figure 1 Main screen of the software controlling AGE-1

The graphitization procedure of AGE comprises 4 main steps (Figure 2). Sample combustion or loading of the CO_2 are relatively short and simple procedures, where only the combustion in the EA and program timing can be tuned. The real benefit in graphite quality and reaction time can be obtained with optimization of the catalyst conditioning and with tuning of the graphitization reaction conditions.

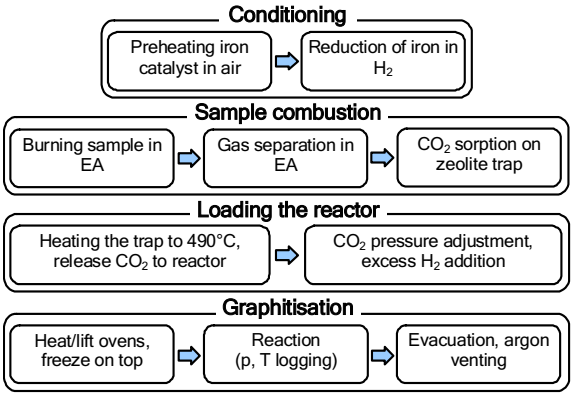

Figure 2 Scheme of the graphitization procedure used

https://doi.org/10.1017/S0033822200046464 Published online by Cambridge University Press

Hardware setup of the trap and reactors used in the device is designed for routine preparation of ~1-mg carbon samples (Wacker et al. 2010). The reactors (Figure 3) are vertically arranged with the reversed cold and heated zones. Such a design should improve heating and mass transport from the heated catalyst at the bottom to the cold "water trap" at the top. From the reaction point of view, AGE reactors are closed systems with volumes of ~4.4 mL designed for pressures up to 1.6 bar.

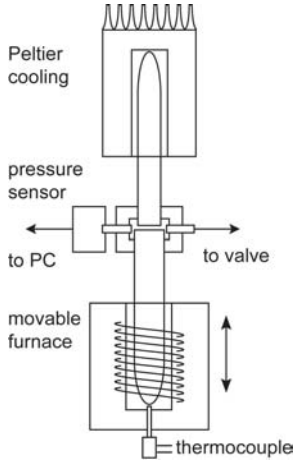

Figure 3 Simplified scheme of graphitization reactor at AGE-1

Pneumatically lifted ovens with a thermocouple sensor in the center of the heating zone are placed under the reactors. During the heating phase, this thermocouple just touches the bottom of the reaction vial. Temperature in the reactor, on the spot where the iron catalyst is placed, is derived from the calibration curve. The calibration procedure uses a reference thermocouple, which can be placed inside on the bottom of the reaction vial. The procedure is programmed for up to 10 calibration points in the range 200–650 °C; each point is obtained as an average over a set time after temperature stabilization.

The absorption trap is a small column filled with 13X zeolite. This material absorbs gases in the following order: $H_2O > CO_2 > O_2 > N_2$. The EA allows separation of combustion gases and also removal of water in the drying column filled with P_2O_5. The AGE program waits until the CO_2 peak occurs and then opens the valve to the zeolite trap. CO_2 from the EA outlet is absorbed in the trap at 25–35 °C; after closing the connection to the EA, the trap is evacuated to remove the rest of the carrier gas. In the loading procedure, the trap is heated for 35 s to 490 °C to release all the CO_2, which then expands to the open reactor. After the loading procedure (Figure 2; Wacker et al. 2010), the trap is evacuated, heated again to 550–570 °C, and flushed with He to remove all traces of CO_2. When the cleaning is finished, the trap is cooled from the outside with compressed air back to the sorption temperature. All these processes—the absorption, loading, and cleaning steps—take 10–15 min depending on the amount of CO_2 in the combusted sample.

In the experiments and in routine operations, the following materials were used:

- Alfa Aesar –325 mesh iron (purity 99%) as a catalyst for graphitization; the iron powder was stored in standard laboratory conditions;
- Hydrogen Lindegas H_2 3.95 as a reduction gas;
- Oxygen Lindegas O_2 5.0 for sample combustion;
- Helium Lindegas He 4.5 as a carrier gas for EA;
- Brown coal ETH No. 34905 as a ^{14}C blank material.

https://doi.org/10.1017/S0033822200046464 Published online by Cambridge University Press

To find the optimal reaction parameters, blank (brown coal) samples were combusted, and the resulting CO_2 was graphitized at various H_2/CO_2 pressure ratios and temperatures. To avoid influence of reactor difference or temperature calibration on the results, all the reactions at the given temperature were realized in the same reactor. For graphitization, a catalyst (3.20 ± 0.06 mg) preheated for 240 s followed with 3-step reduction was used (Figure 6). At the end of the reaction, the reactors were evacuated and flushed with argon to remove all residual gases. Peltier cooling remained switched on until the samples were removed; then, the reactors were evacuated for about 30 min to remove all the water residuals.

Reaction time, shape of reaction curve, water trapping, final pressures, and graphite yield were monitored to characterize the process. Graphitized samples were immediately pressed to the targets and then measured by the MICADAS AMS system to determine the isotopic changes ($\delta^{13}C$) and molecular fragment formation (^{13}CH current).

THEORY

Thermodynamic properties and reactions in the system with iron, hydrogen, and CO_2 are well described in numerous articles related to metallurgy, iron ore treatment, or hydrocarbon production. Unfortunately, these articles are not focused directly on carbon production. Useful information for graphitization processes can be found in the literature (Pichler and Merkel 1949; Walker et al. 1959a,b; Manning and Reid 1977; Sacco and Reid 1979; Liaw and Davis 2000; van der Laan and Beenackers 2000; Gudenau et al. 2005; Oeters et al. 2009).

The graphitization process with hydrogen is rather complex. However, it can be described in a simplified way by a single Bosch reaction:

$$CO_2 + 2H_2 = C + 2H_2O \quad (1)$$

For better understanding of the reaction system and its mechanism, a more detailed view on equilibrium reactions is necessary and their visualization in Baur-Glaessner, Richardson, and similar diagrams (Gudenau et al. 2005; Oeters et al. 2009) is a helpful option (Figure 4). These diagrams describe well the system in equilibrium conditions at a defined pressure. However, a pressure decrease during the graphitization reaction in closed reactors has to be considered.

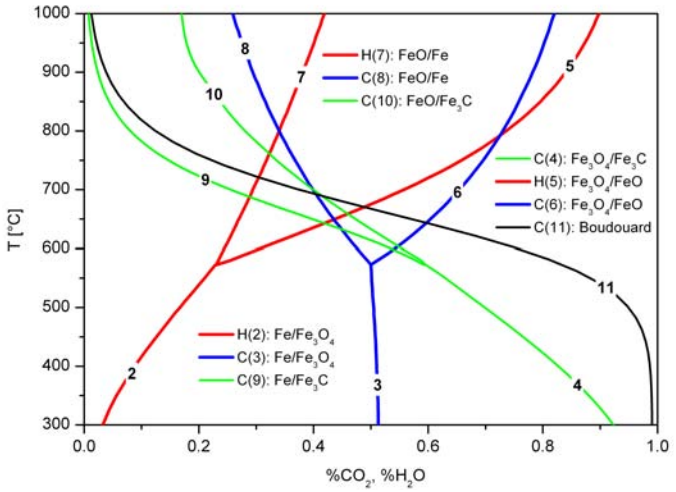

Figure 4 Baur-Glaessner diagram of iron and H_2/H_2O and CO/CO_2 systems at standard pressure. Numbers correspond to the equations in the text.

https://doi.org/10.1017/S0033822200046464 Published online by Cambridge University Press

The iron catalyst plays a very important role in the graphitization system and it is important to understand how it influences the reaction mechanism at given conditions. At temperatures lower than 573 °C and standard pressure, FeO is not stable and only the reactions between magnetite, iron, CO_2, and hydrogen take place. At higher carbon contents, the iron can be transformed to iron carbides or their mixtures with iron or magnetite:

$$Fe_3O_4 + 4H_2 = 3Fe + 4H_2O_{(g)} \quad (2)$$

$$3Fe + 4CO_2 = Fe_3O_4 + 4CO \quad (3)$$

$$Fe_3O_4 + 6CO = Fe_3C + 5CO_2 \quad (4)$$

At temperatures >573 °C, the FeO (wustite) phase occurs and introduces another set of reactions:.

$$Fe_3O_4 + H_2 = 3FeO + H_2O_{(g)} \quad (5)$$

$$Fe_3O_4 + CO = 3FeO + CO_2 \quad (6)$$

$$Fe + H_2O = FeO + H_2 \quad (7)$$

$$Fe + CO_2 = FeO + CO \quad (8)$$

$$3Fe + 2CO = Fe_3C + CO_2 \quad (9)$$

$$3FeO + 5CO = Fe_3C + 4CO_2 \quad (10)$$

When temperatures are <648 °C, iron (ferrite) and its carbides (cementite Fe_3C, Fe_2C and others) are always present. At higher temperatures (up to 723 °C) and carbon content >0.025%, the ferrite with dissolved carbon and cementite are present. The carbon production is strongly influenced by the Boudouard equilibrium:

$$2CO = C_{(s)} + CO_2 \quad (11)$$

Above its curve (see Figure 4), the reaction in the gas phase is shifted to CO. Under the curve, the carbon is deposited and CO_2 is produced. However, its kinetics without a catalyst is quite slow and this reaction practically does not proceed at low CO concentrations and low temperatures. Carbon deposition is strongly enhanced with metallic iron as catalyst, and the reaction runs efficiently in Fe and high CO region.

The presented graphitization reactions can be summarized as follows. Iron reduces the CO_2 to CO and hydrogen reduces the resulting Fe_3O_4 back to Fe (at higher temperatures over FeO). This reduction with hydrogen regenerates Fe in the system and causes the iron to act as a catalyst. Thus, the reaction will run catalyzed until hydrogen, as a reduction agent, is consumed. When no hydrogen is present, iron enters the reactions as the only reducing agent and is consumed to oxides and then conditionally to carbides. This means that sufficient hydrogen has to be present for fast and complete graphitization, and its deficiency leads to slow or incomplete reaction.

On the other hand, too much hydrogen is also undesirable. The disadvantage of hydrogen reduction is its reaction with carbon compounds to unwanted hydrocarbons:

$$C + 2H_2 = CH_4 \quad (12)$$

$$Fe_3C + 2H_2 = 3Fe + CH_4 \quad (13)$$

$$Fe_3C + 4H_2O = Fe_3O_4 + 2H_2 + CH_4 \quad (14)$$

https://doi.org/10.1017/S0033822200046464 Published online by Cambridge University Press

These reactions decrease the yield of carbon; the final ratio between C and CH_4 is mostly determined by temperature and a related point on the methane decomposition curve (see Figure 5 for reaction 12); the yields of hydrocarbons are usually lower at higher temperatures.

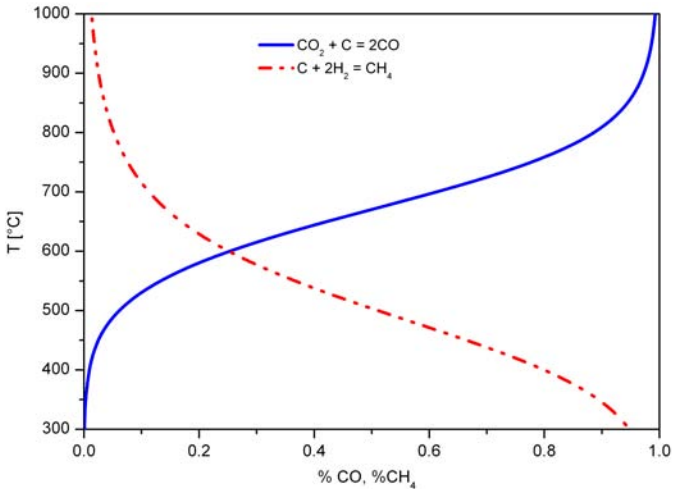

Figure 5 Boudouard (11) and methanization (12) equilibrium curves

The H_2/H_2O ratio is crucial for carbon and iron compounds reduction as well as for the hydrocarbons production. In all the above reactions, water is the final product of hydrogen oxidation and its pressure determines the equilibrium according to the Le Chatelier principle—the water trapping during graphitization significantly shifts the equilibrium, increasing the reaction rate and the yield of carbon. All the water-gas reactions (homogenous and heterogenous) and homogenous methane synthesis are strongly influenced by water pressure as well:

$$CO + H_2O_{(g)} = CO_2 + H_2 \quad (15)$$

$$C_{(s)} + H_2O_{(g)} = CO + H_2 \quad (16)$$

$$C_{(s)} + 2H_2O_{(g)} = CO_2 + 2H_2 \quad (17)$$

$$CO + 3H_2 = CH_4 + H_2O \quad (18)$$

These reactions run faster in the presence of a catalyst like iron.

The behavior of carbon on the iron surface during graphitization process is well described in Sacco et al. (1984) and Liaw and Davis (2000). They assume that initially deposited carbon diffuses into the iron structure, forming the cementite phase. This process corrupts the catalyst surface and, consequently, the filamentous carbon starts growing on the transformed surface.

RESULTS AND DISCUSSION

Sample Combustion

Sample combustion in the EA was tuned to be fast while maintaining a good separation of the combustion gases N_2 and H_2O from CO_2. Water was removed directly from the gas with a column filled with P_2O_5 (Sicapent™ or P_2O_5 with moisture indicator, Fluka). Various carrier gas flows were tested

https://doi.org/10.1017/S0033822200046464 Published online by Cambridge University Press

to achieve optimum CO_2 peak timing. Finally, the flow 150 mL min^{-1} of He carrier gas was used, then the combustion procedure time from sample throw-in to the end of CO_2 peak took ~10 min. The efficiency of sample transport from the EA to the reactor is about 92% and is summarized in Table 1. The small trap volume causes some small sample losses because the CO_2 is only expanded into the reactors from the trap (and not frozen over).

Table 1 Average values[a] of CO_2 transport efficiency from elemental analyzer (EA) to reactor.

Sample type	Average sample weight (mg)	Carbon measured (%)	pCO_2 in reactor (mbar)	Efficiency of CO_2 transport (%)
Oxalic acid	5.452 ± 0.068	18.81 ± 0.17	446.0 ± 6.8	92.7 ± 2.3
Coal	1.337 ± 0.037	85.22 ± 1.11	490.1 ± 16.2	91.7 ± 4.5

[a]Average values of 25 oxalic acid and 55 brown coal sample combustions related to the same EA calibration curve.

Catalyst Pretreatment

Iron preheating with hydrogen at temperatures 350–600 °C is a widely used catalyst pretreatment procedure. Its purpose is to reduce any oxide surface layer to iron and also to remove tracers of contaminants such as carbon (adsorbed CO_2, carbonates, carbides, etc.), sulfur (catalytic poison), etc. However, in case of high oxide and adsorbed water content on the iron and when the reducing temperature is too low or the content of formed water too high, it may then happen that the oxide (magnetite at <573 °C) is only redispersed towards the catalyst surface. This will result in slow reaction and additional hydrogen consumption during the graphitization process. We propose a catalyst pretreatment with a first short oxidation of the iron surface followed by reduction with hydrogen (Figure 6). The oxidation transforms the catalyst to a well-defined state. Impurities on the surface are oxidized to volatile oxides (e.g. CO_2, SO_2) and water is desorbed. These resulting gases can be easily pumped off.

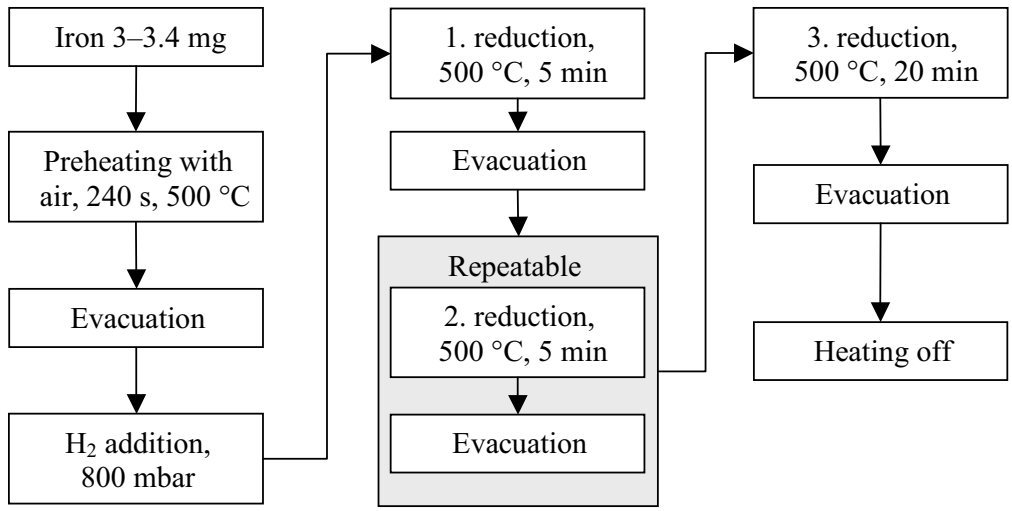

Figure 6 Catalyst pretreatment scheme

Next, the iron catalyst is reduced back to iron with hydrogen at 500 °C. Here, it is necessary to keep the $H_2/(H_2 + H_2O)$ close to 1 or at a known certain H_2/H_2O ratio using the temperature above equilibrium curve of reaction 2 (see the Baur-Glaessner diagram, Figure 4).

https://doi.org/10.1017/S0033822200046464 Published online by Cambridge University Press

To remove any formed water or gases from the remaining contaminants, the reactors are evacuated and refilled with hydrogen after 5 and 10 min. The reducing treatment with hydrogen is finished after a 20-min-long third step (Figure 6). The success of pretreatment can be checked visually—the resulting catalyst (Fe) color still has to be metallic-gray, while magnetite is black.

The oxidation-reduction steps result in catalyst surface changes and likely increase the surface, which then influence the reaction rate. An oxidation of 4 min at 500 °C with air was tested to give good results, whereas a short or even no oxidation produced a very variable and long graphitization time (Table 2).

Table 2 Average reaction times at various catalyst preheating time ($T_{preheating}$ = 400 °C, $T_{reaction}$ = 570 °C, H_2/CO_2 ratio = 2.3).

Preheating (s)	Average reaction time (hr)
0	3.3
30	2.9
60	1.9
90	1.4
120	1.4

Graphitization Reaction

In Figures 7a–e, the reaction curves at various H_2/CO_2 ratios and temperatures are shown. The differences in reaction curve shapes among reactions are significant; especially at higher H_2/CO_2 ratios the curves shows additional wiggles and the gradual process at the beginning no longer occurs at higher temperatures.

Final pressure values after a 140-min reaction and a comparison with theoretical values, calculated from the H_2/CO_2 stoichiometric ratio in Bosch reaction (1), are shown in Table 3. All the relative pressures were recalculated to laboratory temperature (25 °C) and related to initial filling pressure. From the reaction curves and related final pressures, the following observations can be summarized:

- The lowest final pressures were obtained for 2.1–2.3 H_2/CO_2 ratios and temperature range 580–600 °C. The measured and calculated pressures are similar at these conditions and the variations are in the range of only 1.5–2.5% of the filling pressure.
- Final pressure at all H_2/CO_2 ratios is much lower than simply estimated from the excess of hydrogen (reaction 1). An explanation can be found in the methane production (e.g. reaction 12), where 2 moles of hydrogen react to form 1 mole of methane. This trend is more significant at the highest ratio, when the pressure differences are much higher at lower temperatures.

Table 3 Relative final pressures (%) (related to initial total pressure at standard temperature of 25 °C) of graphitization reaction after 140 min (measured/assumed from Bosch reaction 1).

Ratio H_2/CO_2	540 °C	560 °C	580 °C	600 °C	620 °C
1.8	4.9/6.2	4.4/7.2	5.0/7.0	4.0/6.4	4.4/5.4
2.1	3.1/4.6	2.2/4.6	2.2/4.0	2.0/3.6	2.5/4.7
2.3	2.9/9.7	2.3/9.2	2.1/9.7	2.1/9.3	3.8/9.4
2.5	3.5/15.0	3.9/15.0	3.8/15.2	4.0/15.2	5.0/14.9

https://doi.org/10.1017/S0033822200046464 Published online by Cambridge University Press

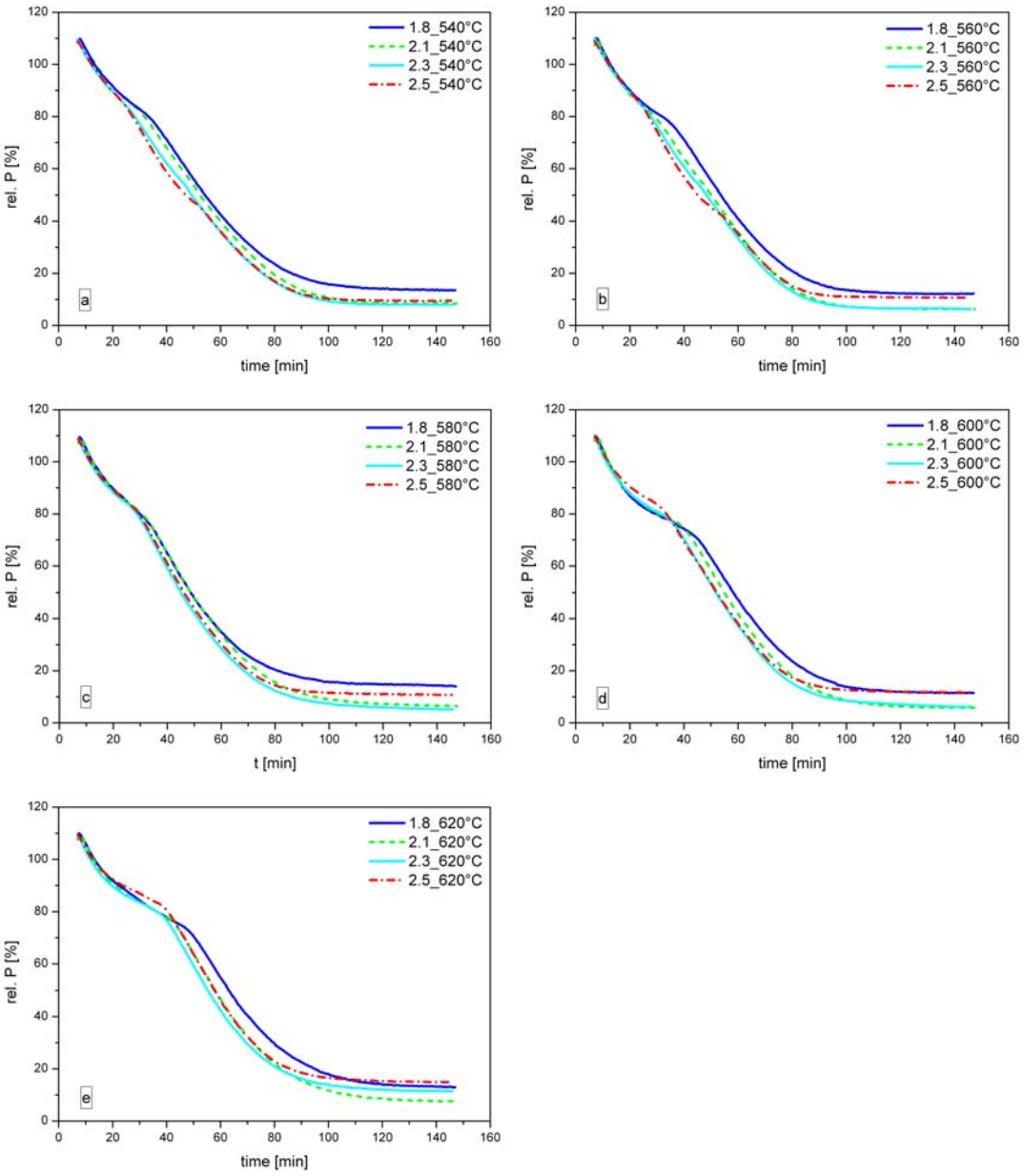

Figure 7a–e Pressure record of graphitization reactions at various temperatures and H_2/CO_2 ratios

Comparison of the optimized and the original reaction shows a significant difference in reaction time (Figure 8 and Figure 9A and D). The curves B and C show the influence of cooling on the reaction process. In the optimized system (curve A), water is frozen at −10 °C and its vapor pressure above ice at this temperature is about 2.6 mbar.

https://doi.org/10.1017/S0033822200046464 Published online by Cambridge University Press

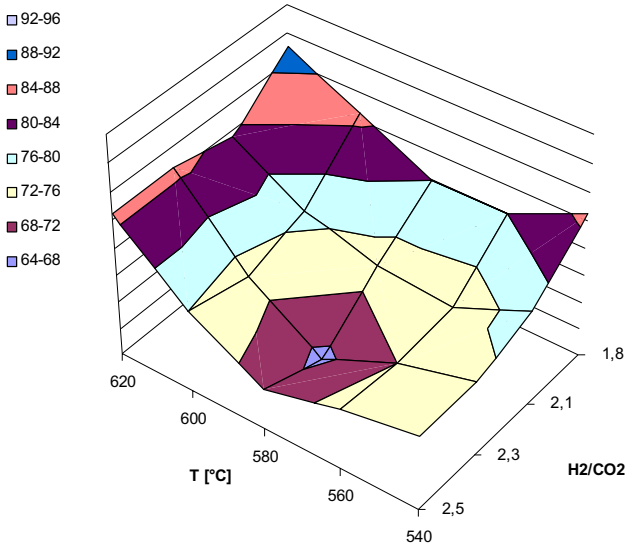

Figure 8 Reaction time coefficients (min) of graphitization process at tested temperature and H_2/CO_2 ratios. (The coefficients were determined artificially as an extension of the linear part of the curve to the final pressure and are used here only as an indicator of reaction rate.)

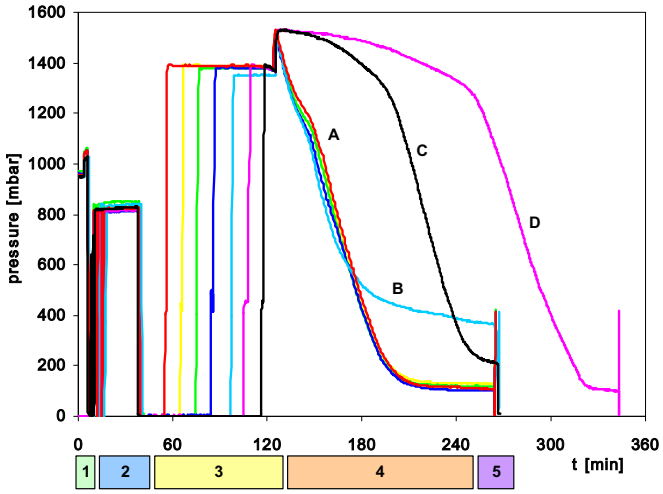

Figure 9 Record of the whole graphitization procedure (1-catalyst preheating, 2-reduction by H_2, 3-reactor loading, 4-reactions, 5-flushing with Ar): A) optimized reaction; B) water trap cooled to laboratory temperature; C) no cooling; D) not optimized reaction without catalyst pretreatment.

Quality of Graphite

The isotopic changes ($\delta^{13}C$) and molecular fragment formation (^{13}CH current) of the graphitized samples measured with MICADAS are given in Figures 10 and 11. The "normalized ^{13}CH current" variable used for process description is the ^{13}CH current measured by MICADAS normalized to the ^{12}C current of the same sample. For such purposes, all the samples were measured at the same stable device settings.

The normalized ^{13}CH currents decline with increasing graphitization temperature from 1.2 to 0.4 μA for all H_2/CO_2 ratios; the average ^{12}C current was 13.1 ± 0.5 μA. These results together with residual pressures can be interpreted as a strong decrease in production of methane and other hydrocarbons at high temperatures. The sorption of methane (boiling point –161.6 °C) on iron catalyst is not supposed to be high at laboratory or higher temperatures, so probably some heavier hydrocarbons may be produced or there may exist a strong methane sorption on the produced carbon.

https://doi.org/10.1017/S0033822200046464 Published online by Cambridge University Press

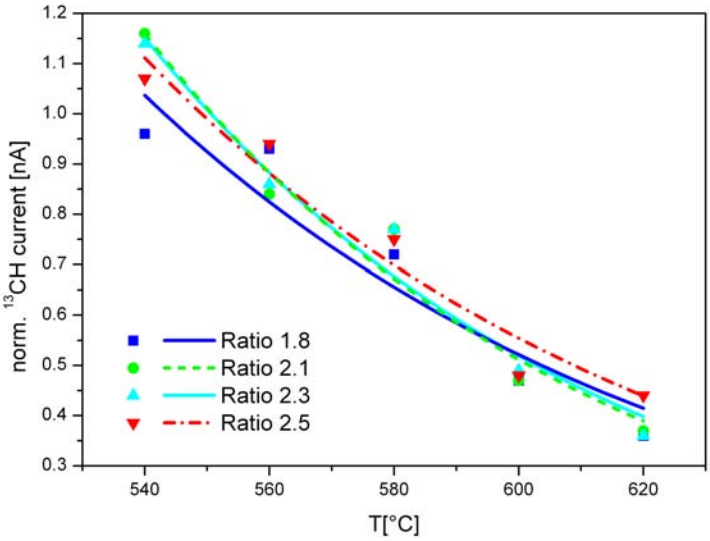

Figure 10 Normalized ^{13}CH current (nA) of samples graphitized at various temperatures and H_2/CO_2 ratios.

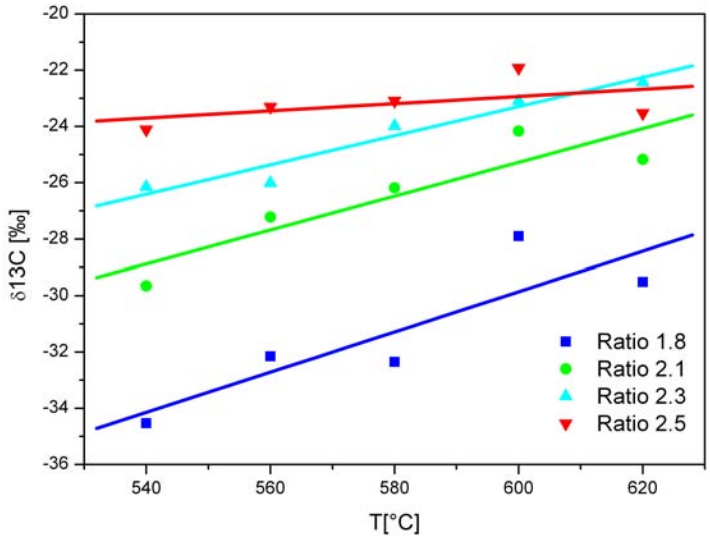

Figure 11 δ^{13}C changes in samples prepared at various temperatures and H_2/CO_2 ratios

The isotopic fractionations in Figure 11 show large shifts at lower H_2/CO_2 ratios and temperatures towards lower ratios. Such isotopic shifts are generally accepted as an indication of an incomplete reaction. This suggestion also corresponds to the reaction graphs (Figure 7), where also the shape of the reaction curves at the lowest 1.8 ratio shows that the reactions were not completed in 140 min at all tested temperatures. Additionally, the lower $^{13}C/^{12}C$ values at lesser temperatures can be explained by the creation of hydrocarbons, when during reactions between gas and solid compounds (e.g. reaction 12) isotopic effects may occur.

https://doi.org/10.1017/S0033822200046464 Published online by Cambridge University Press

Based on the AMS results, optimum reaction conditions were chosen as a compromise on all measured trends. The isotopic fractionation and molecular current are strongly depressed at higher temperatures. High H_2/CO_2 ratios provide better reaction completion, but slightly increase molecular currents. On the other hand, the reaction takes longer at low (540 °C) and also high (620 °C) temperatures and the shortest reaction time was found around 580 °C and a ratio of 2.3. The final parameters used are summarized in Table 4. The reaction time was set to 140 min; this time was successfully used in the testing phase and it is long enough to achieve reaction completion.

Table 4 Major parameters of AGE graphitization procedure.

Reactor volume 4.4 mL	Carbon mass in Fe ~0.9 mg
Trap volume 0.4 mL	H_2/CO_2 ratio 2.3
Iron weight 3–3.5 mg	Reaction temperature 590 °C
Iron conditioning 500 °C, 240s (air), 5 + 5 + 20 min (H_2)	Average blank value <0.3 pMC
CO_2 pressure 420 mbar	Reaction time 140 min[a]

[a]140 min is used in routine operation to support reaction completion.

With the parameters chosen, the set of samples was graphitized to determine the carbon yield and the reaction changes at various catalyst amounts. The amount of total carbon in the reactor was calculated from the CO_2 pressure; carbon mass was determined by iron weight difference before and after the reaction. The results in Figure 12 show that the ^{12}C current correlates to the C/Fe ratio in the target and that the carbon amount on the iron is practically constant. This implies that the carbon yield of the reaction does not depend on the iron quantity in the tested range. No significant changes in $^{13}C/^{12}C$ measured ratios (Figure 13) were observed; this can be interpreted that completion of the reaction is not influenced by the catalyst quantity in the tested Fe/C ratio region. Any changes in pMC values of the blank with the increasing iron amount could not be determined.

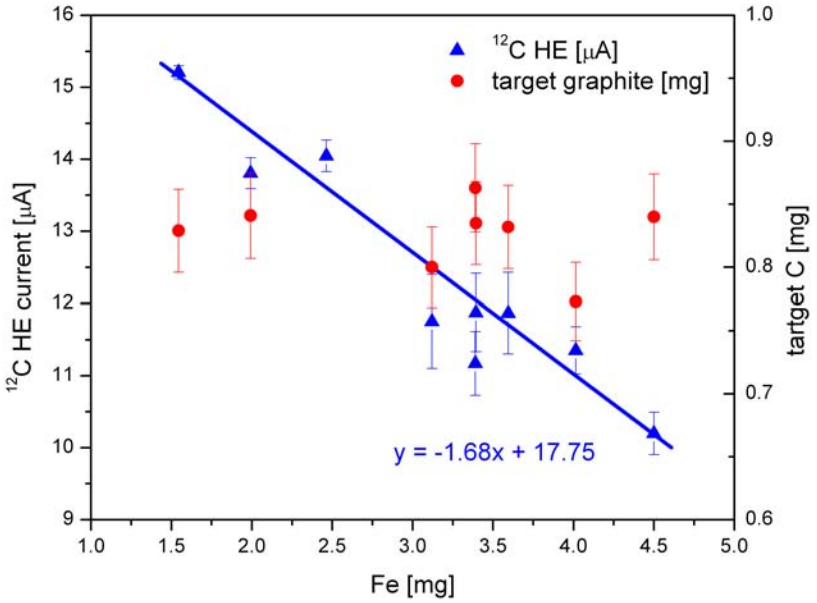

Figure 12 ^{12}C current (μA) and target C amount (mg) at various catalyst quantities (mg)

https://doi.org/10.1017/S0033822200046464 Published online by Cambridge University Press

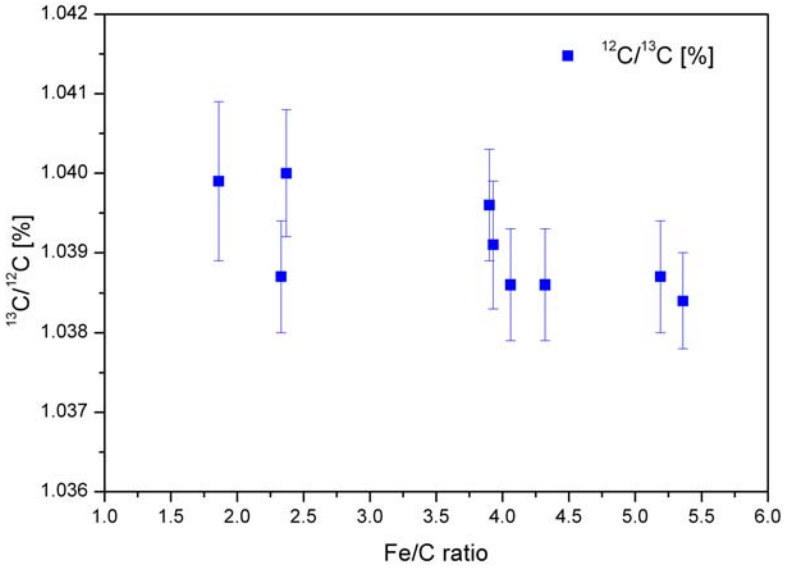

Figure 13 Changes in $^{13}C/^{12}C$ ratio (%) of prepared blank samples at various Fe/C ratios

The average final carbon mass of 0.85 mg over all tested samples corresponds to approximately 95% reaction yield. Together with the transport efficiency of ~92%, the total efficiency of the graphitization procedure in carbon production is about 88%.

SUMMARY

Optimization of reaction conditions and catalyst pretreatment resulted in a significant improvement of the graphitization process and our findings can be well described by thermodynamic data. The graphitization reaction itself last now <90 min. A significant influence of temperature and H_2/CO_2 ratio on the produced graphite quality was observed as well as a positive influence of oxidative catalyst pretreatment. A 95% carbon yield in the optimized reaction and 92% efficiency of the CO_2 transport to the reactors were determined; these values result in a high value of 88% overall (sample—target graphite) procedure efficiency. At these optimum conditions, the carbon yield and quality is not influenced by the catalyst amount in the 1.5–4.5 mg Fe range.

REFERENCES

Dee M, Bronk Ramsey C. 2000. Refinement of graphite target production at ORAU. *Nuclear Instruments and Methods in Physics Research B* 172(1–4):449–53.

Gudenau HW, Senk D, Wang SW, Martins KD, Stephany C. 2005. Research in the reduction of iron ore agglomerates including coal and C-containing dust. *ISIJ International* 45(4):603–8.

Jull AJT, Donahue DJ, Hatheway AL, Linick TW, Toolin LJ. 1986. Production of graphite targets by deposition from CO/H_2 for precision accelerator ^{14}C measurements. *Radiocarbon* 28(2A):191–7.

Liaw S-J, Davis BH. 2000. Fischer-Tropsch synthesis. Compositional changes in an iron catalyst during activation and use. *Topics in Catalysis* 10(1–2):133–9.

Manning MP, Reid RC. 1977. C-H-O systems in presence of an iron catalyst. *Industrial & Engineering Chemistry Process Design and Development* 16:358–61.

McNichol AP, Gagnon AR, Jones GA, Osborne EA. 1992. Illumination of a black box: analysis of gas composition during graphite target preparation. *Radiocarbon* 34(3):321–9.

Oeters F, Ottow M, Senk D, Beyzavi A, Güntner J, Lüngen HB, Koltermann M, Buhr A, Yagi J, Formanek L. 2009. Iron. In: *Ullmann's Encyclopedia of Industrial Chemistry.* Weinheim: Wiley-VCH. 178 p.

Pichler H, Merkel H. 1949. Chemical and thermomagnetic studies on iron catalysts for synthesis of hydro-

https://doi.org/10.1017/S0033822200046464 Published online by Cambridge University Press

carbons. Washington, DC: US Bureau of Mines. p 16–27.

Sacco A, Reid RC. 1979. Water limitation in the C-H-O system over iron. *AIChE Journal* 25(5):839–43.

Sacco A, Thacker P, Chang TN, Chiang ATS. 1984. The initiation and growth of filamentous carbon from alpha-iron in H_2, CH_4, H_2O, CO_2, and CO gas mixtures. *Journal of Catalysis* 85:224–36.

Santos GM, Southon JR, Griffin S, Beaupre SR, Druffel ERM. 2007. Ultra small-mass AMS ^{14}C sample preparation and analyses at KCCAMS/UCI Facility. *Nuclear Instruments and Methods in Physics Research B* 259(1):293–302.

Slota Jr PJ, Jull AJT, Linick TW, Toolin LJ. 1987. Preparation of small samples for ^{14}C accelerator targets by catalytic reduction of CO. *Radiocarbon* 29(2):303–6.

Synal H-A, Stocker M, Suter M. 2007. MICADAS: a new compact radiocarbon AMS system. *Nuclear Instruments and Methods in Physics Research B* 259(1): 7–13.

van der Laan GP, Beenackers AACM. 2000. Intrinsic kinetics of the gas-solid Fischer-Tropsch and water gas shift reactions over a precipitated iron catalyst. *Applied Catalysis A* 193(1–2):39–53.

Verkouteren RM, Klinedinst DB, Currie LA. 1997. Iron-manganese system for preparation of radiocarbon AMS targets: characterization of procedural chemical-isotopic blanks and fractionation. *Radiocarbon* 39(3):269–83.

Vogel JS. 1992. Rapid production of graphite without contamination for biomedical AMS. *Radiocarbon* 34(3):344–50.

Vogel JS, Southon JR, Nelson DE, Brown TA. 1984. Performance of catalytically condensed carbon for use in accelerator mass spectrometry. *Nuclear Instruments and Methods in Physics Research B* 5(2):289–93.

Vogel JS, Nelson DE, Southon JR. 1987a. ^{14}C background levels in an accelerator mass-spectrometry system. *Radiocarbon* 29(3):323–33.

Vogel JS, Southon JR, Nelson DE. 1987b. Catalyst and binder effects in the use of filamentous graphite for AMS. *Nuclear Instruments and Methods in Physics Research B* 29(1–2):50–6.

Wacker L, Němec M, Bourquin J. 2010. A revolutionary graphitisation system: fully automated, compact and simple. *Nuclear Instruments and Methods in Physics Research B* 268(7–8):931–4.

Walker Jr PL, Rakszawski JF, Imperial GR. 1959a. Carbon formation from carbon monoxide-hydrogen mixtures over iron catalysts. 1. Properties of carbon formed. *Journal of Physical Chemistry* 63(2):133–40.

Walker Jr PL, Rakszawski JF, Imperial GR. 1959b. Carbon formation from carbon monoxide-hydrogen mixtures over iron catalysts. 2. Rates of carbon formation. *Journal of Physical Chemistry* 63(2):140–9.

Xu XM, Trumbore SE, Zheng SH, Southon JR, McDuffee KE, Luttgen M, Liu JC. 2007. Modifying a sealed tube zinc reduction method for preparation of AMS graphite targets: reducing background and attaining high precision. *Nuclear Instruments and Methods in Physics Research B* 259(1):320–9.

Yoneda M, Shibata Y, Tanaka A, Uehiro T, Morita M, Uchida M, Kobayashi T, Kobayashi C, Suzuki R, Miyamoto K, Hancock B, Dibden C, Edmonds JS. 2004. AMS ^{14}C measurement and preparative techniques at NIES-TERRA. *Nuclear Instruments and Methods in Physics Research B* 223–224:116–23.